Fully Conjugated Graft Copolymers Comprising a P-Type Donor– Acceptor Backbone and Poly(3-hexylthiophene) Side Chains Synthesized Via a "Graft Through" Approach

ARTICLE *in* MACROMOLECULES · JULY 2014

Impact Factor: 5.8 · DOI: 10.1021/ma5009435

3 AUTHORS, INCLUDING:

Katherine A Mazzio
Helmholtz-Zentrum Berlin
11 PUBLICATIONS **126** CITATIONS
SEE PROFILE

Christine Luscombe
University of Washington Seattle
62 PUBLICATIONS **2,267** CITATIONS
SEE PROFILE

Macromolecules

Article

pubs.acs.org/Macromolecules

Fully Conjugated Graft Copolymers Comprising a P-Type Donor–Acceptor Backbone and Poly(3-hexylthiophene) Side Chains Synthesized Via a "Graft Through" Approach

David F. Zeigler,[†] Katherine A. Mazzio,[‡] and Christine K. Luscombe*[,†,‡]

[†]Department of Chemistry and [‡]Department of Materials Science and Engineering, University of Washington, Seattle, Washington 98195-2120, United States

Supporting Information

ABSTRACT: A series of fully conjugated graft copolymers containing poly(3-hexylthiophene) (P3HT) side chains and a p-type carbazole-diketopyrrolopyrrole (CbzDPP) donor–acceptor backbone were synthesized via a graft through Suzuki polymerization. The macromonomers were formed by externally initiating P3HT growth from a boronic ester-functionalized carbazole via Kumada catalyst transfer polycondensation. Subsequently, this macromonomer was copolymerized with a DPP monomer via a graft through Suzuki polymerization to yield the final graft copolymers. The graft copolymers exhibit optical and electronic properties of both P3HT and the CbzDPP polymers independently due to the break in conjugation between the carbazole unit and P3HT chain. Moreover, these properties reflect the relative proportion of P3HT and CbzDPP polymers; shorter P3HT chain lengths lead to graft copolymers that possess more CbzDPP character and vice versa. The macromonomers were characterized by gel permeation chromatography, mass spectrometry, and UV–visible spectroscopy. The graft copolymers were further investigated using gel permeation chromatography, UV–visible spectroscopy, cyclic voltammetry, differential scanning calorimetry, and atomic force microscopy. Finally, organic field effect transistors were fabricated using the graft copolymers and compared to an analogous linear CbzDPP copolymer. Ultimately, the graft copolymers with the longest P3HT chains (ca. 75 repeat units) exhibited almost exclusively P3HT characteristics, possessing a small CbzDPP internal charge transfer (ICT) peak and only p-type conductivity ($\mu_h \sim 6 \times 10^{-4}$ cm^2 V^{-1} s^{-1}). Conversely, the graft copolymers with the shortest P3HT chains (ca. 10 repeat units) showed significant CbzDPP character, including a strong ICT peak and ambipolar mobilities ($\mu_h \sim 5 \times 10^{-3}$ cm^2 V^{-1} s^{-1}; $\mu_e \sim 7 \times 10^{-4}$ cm^2 V^{-1} s^{-1}).

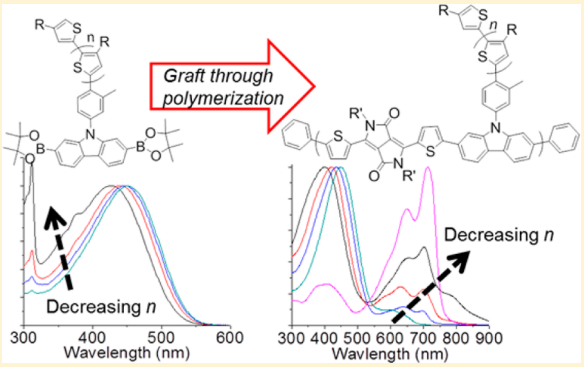

INTRODUCTION

Although the efficiencies of organic photovoltaics (OPV) are increasing, one drawback of conjugated organic molecules is that they tend to have narrow absorption bandwidths, leading to losses from some combination of excitonic thermalization or sub-bandgap transmission.[1,2] The former occurs when an electron is excited beyond the lowest occupied molecular orbital (LUMO) of the donor and relaxes toward the LUMO during exciton diffusion by releasing energy in the form of photons or phonons. The latter results when photons with energies smaller than the bandgap of the donor are transmitted through the device; this is a direct consequence of the requirements for energy level alignment between the donor, acceptor, and electrodes to achieve efficient charge transfer between materials, which places a finite limit on the size of the donor band gap.

One strategy to address these problems simultaneously is to utilize a tandem solar cell, which is composed of two (or more) photovoltaic cells, typically connected in series.[3−12] These two cells possess donor/acceptor materials that exhibit complementary absorption spectra to cover the majority of the visible spectrum; generally, poly(3-hexylthiophene) (P3HT) is used in conjunction with a smaller band gap donor. Any higher energy photons are absorbed by P3HT, thereby limiting thermalization losses; conversely, any lower energy photons are absorbed by the low band gap material, which alleviates sub-band gap transmission. However, introducing an interconnecting layer between the two cells introduces loss mechanisms and resistances. In addition, since the cells are connected in series, the J_{SC} is limited by the lower J_{SC} of the two cells. As a result, tandem OPVs are achieving similar champion efficiencies (10.6%)[13] to single-junction OPVs (∼10%).[14]

Another strategy to address transmission and thermalization losses without the complicated fabrication inherent to tandem OPVs is to use a ternary blend of materials in a single-junction bulk heterojunction (BHJ).[15−20] This method involves adding both a small band gap donor and a wide band gap donor to an n-type acceptor, which is intended to extend the absorption

Received: May 7, 2014
Revised: July 18, 2014

   dx.doi.org/10.1021/ma5009435 | Macromolecules XXXX, XXX, XXX–XXX

window of the BHJ and thereby improve photon harvesting and the overall J_{SC} of the device. In addition, having a cascade of energy levels in the three BHJ materials has been shown to enhance exciton dissociation efficiencies, which is another major hindrance to achieving high PCE values in OPVs.[21] Such devices have exhibited impressive performances compared to control cells composed of the basis donor materials.[22]

However, conjugated polymers also suffer from inherently low dielectric constants compared to inorganic materials. Thus, polymers generate excitons (Coulombically bound electron−hole pairs) upon light absorption, whereas inorganic materials yield free charge carriers.[23] To form free charge carriers, excitons must diffuse through the polymer phase to a donor−acceptor interface, where the energetic offset in LUMO levels leading to exciton dissociation. Unfortunately, the diffusion length of an exciton is small (ca. 10 nm), which means that recombination is a major loss pathway in OPVs. So far, nanostructured active layers with domain sizes on the order of the exciton diffusion length are the best method to mitigate this loss; the BHJ architecture has remained the most practical way to maximize exciton dissociation efficiency.[24] There have been attempts to covalently bond p- and n-type materials through conjugated and aliphatic chains to achieve better exciton separation efficiencies.[25,26] Like ternary blends, creating a covalent, conjugated linkage between two electronically active materials with sufficiently offset energy levels could enhance exciton dissociation via stepwise charge separation, but without having to rely on random exciton diffusion processes to promote exciton dissociation. Moreover, if these two materials had complementary absorption profiles, thermalization and sub-band gap transmission issues could simultaneously be mitigated. To the best of our knowledge, there have been no reports of direct conjugation between two covalently linked p-type polymers with complementary absorption.

The following studies were predicated on the idea that it is possible to functionalize a low-band gap p-type donor−acceptor (D−A) polymer with P3HT chains to yield a fully conjugated graft copolymer that has broadband absorbance across the visible spectrum and can exhibit enhanced stepwise exciton dissocation. Also of interest was the largely unexplored synthetic chemistry for creating such a polymer, as well as the eventual effects on the optoelectronic characteristics of the final polymer.

Herein, a fully conjugated graft copolymer comprised of a carbazole (Cbz)/diketopyrrolopyrrole (DPP) backbone and P3HT side chains is reported (Figure 1). The polymer was synthesized via a "graft through" approach, wherein a series of boronic ester-functionalized Cbz-P3HT macromonomers with different degrees of P3HT polymerization were synthesized and subsequently polymerized with a DPP comonomer by a Suzuki coupling reaction. The physical, optical, and electrochemical properties of the macromonomers and resultant graft copolymers are reported, as well as organic field effect transistor (OFET) performances.

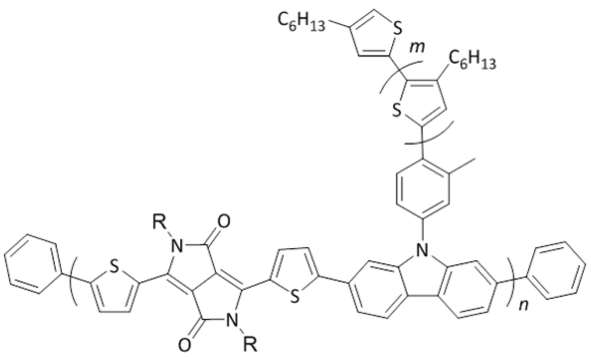

Figure 1. Target conjugated graft copolymer structure.

EXPERIMENTAL SECTION

Materials and Characterization. Unless otherwise specified, all chemicals were purchased from Aldrich and used without further purification. Solvents for synthesis were purified by distillation. All chemical reactions were carried out in a nitrogen atmosphere. 2,7-dibromocarbazole,[27] 1-iodo-2-octyldodecane,[28] 3,6-bis(5-bromothiophen-2-yl)-2,5-bis(2-octyldodecyl)pyrrolo[3,4-*c*]pyrrole-1,4(2*H*,5*H*)-dione[29] and 9-phenyl-2,7-dibromocarbazole[27] were prepared according to published procedures. UV−vis spectra were tested using a PerkinElmer Lambda-9 spectrophotometer. ^{1}H NMR and ^{13}C NMR spectra were collected on Bruker AV 300 or 500 spectrometers operating at 300 or 500 MHz in deuterated chloroform solution with TMS as reference. Polymer molecular weights were measured by a Waters 1515 gel permeation chromatograph (GPC) with a refractive index detector at room temperature (THF as the eluent). Cyclic voltammetries of polymer films were conducted on a BAS CV-50W voltammetric system with a three-electrode cell in acetonitrile with 0.1 M of tetrabutylammonium hexafluorophosphate (Bu_4NPF_6) using a scan rate of 50 mV·s^{-1}. ITO, Ag/AgCl, and Pt wire were used as working electrode, reference electrode and counter electrode, respectively. Differential scanning calorimetry was performed with a TA Instruments Auto Q20 using a heating rate of 10 °C/min. All AFM images were recorded in tapping mode on a Nanoscope II Scanning Probe Microscope (Digital Instruments). All spectra were plotted using OriginPro 8. A reaction scheme is shown in Scheme 1.

OFET Device Fabrication. Organic field-effect transistors (OFETs) were fabricated in a top-contact bottom-gate device geometry on heavily doped p-type silicon ⟨100⟩ wafers with a 300 nm thermal oxide layer, purchased from Montco Silicon Technologies. Substrates were cleaned by sequential ultrasonication twice with fresh acetone, followed by isopropyl alcohol for 15 min each. They were then dried under a stream of nitrogen and treated by air plasma for 15 min before passivating the oxide layer with a thin divinyltetramethyldisiloxane−bis(benzocyclobutene) (BCB, Dow Chemicals, Inc.) buffer layer. A precursor solution of 1 wt % BCB in toluene was spin coated in air at 4000 rpm for 60 s on the oxide layer. The substrates were subsequently annealed at 250 °C overnight in a glovebox. Solutions of each polymer were prepared in chloroform ($CHCl_3$) and chlorobenzene (CB) at concentrations of 5 mg/mL and allowed to stir in a glovebox overnight before filtering with a 0.2 um PTFE filter. Filtered solutions were then spin coated on BCB passivated substrates at 2000, 3000, or 4000 rpm for 60 s. The best device performances were found for OFETs made in $CHCl_3$ and spin coated at 2000 rpm. These thin films were annealed at 65, 95, 125, and 155 °C for 10 min under nitrogen prior to electrode deposition in order to determine their optimal device performance conditions. Gold source and drain electrodes were thermally evaporated through a shadow mask at a base pressure of 7×10^{-7} Torr at a rate of 1 Å/s to a thickness of 50 nm. The output and transfer characteristics of all transistors were measured in a nitrogen atmosphere using an Agilent 4155B semiconductor parameter analyzer. The field-effect mobility (μ) was determined from a linear fit of $(I_{ds})^{1/2}$ vs V_{gs} in the saturation regime. The threshold voltage (V_t) was estimated from the x-intercept of the linear region of $(I_{ds})^{1/2}$ vs V_{gs}. All devices had a channel length of 100 μm and a width of 1000 μm.

Synthesis of 2,7-Dibromo-9-(4-chloro-3-methylphenyl)-9*H*-carbazole (1). 2,7-Dibromocarbazole (1.56 g, 4.8 mmol), 1-chloro-4-iodo-2-methylbenzene (3.65 g, 14.5 mmol), copper(I) iodide (0.14 g, 0.7 mmol), 1,10-phenanthroline (0.13 g, 0.7 mmol), and potassium carbonate (1.00 g, 7.2 mmol) were added to a 100 mL one-neck flask. Then, DMF (20 mL) was added and the mixture was warmed to 125

dx.doi.org/10.1021/ma5009435 | *Macromolecules* XXXX, XXX, XXX−XXX

Scheme 1. Reaction Scheme[a]

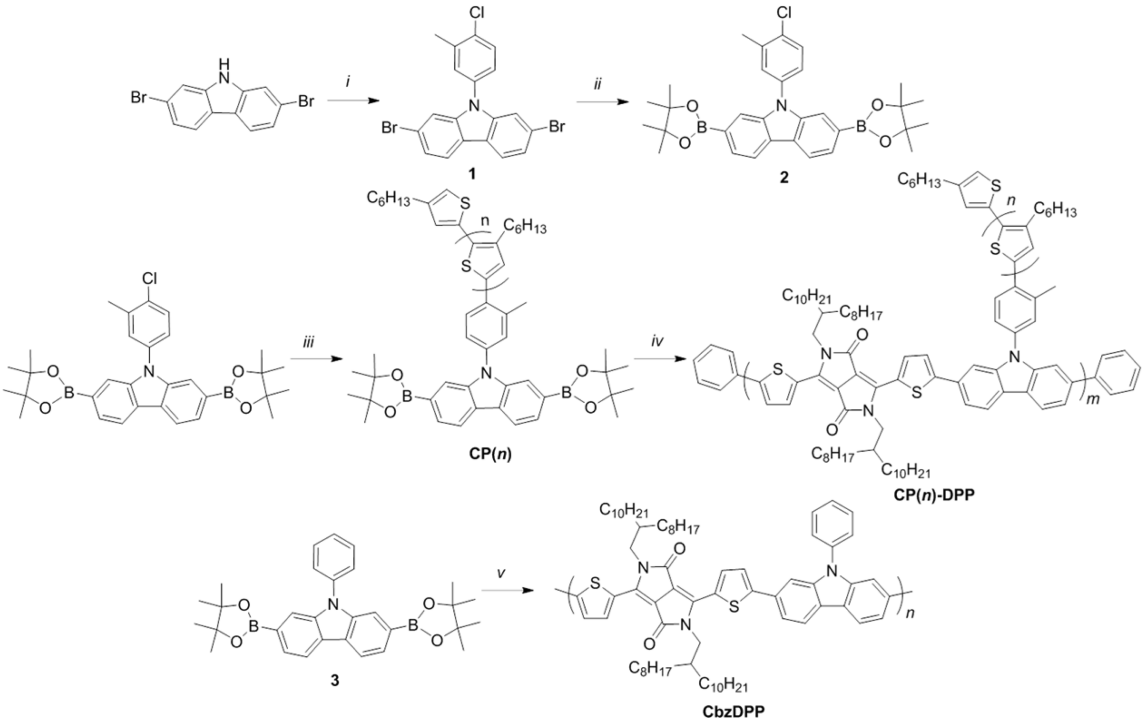

[a](*i*) CuI, 1-chloro-4-iodo-2-methylbenzene, 1,10-phenanthroline, K_2CO_3, DMF, 125 °C, 16 h, 38%; (*ii*) (a) *n*-BuLi, THF, −78 °C, 1 h and (b) 2-isopropoxy-4,4,5,5-tetramethyl-1,3,2-dioxaborolane, room temperature, overnight, 76%; (*iii*) (a) $Ni(COD)_2$, PPh_3, toluene, 50 °C, 3 d, (b) 1,3-bis(diphenylphosphino)propane, room temperature, 3 h, and (c) 2-bromo-5-magnesium chloride-3-hexylthiophene; (*iv*) (a) 3,6-bis(5-bromothiophen-2-yl)-2,5-bis(2-octyldodecyl)pyrrolo[3,4-*c*]pyrrole-1,4(2*H*,5*H*)-dione, 18-crown-6, Aliquat 336, $Pd(PPh_3)_4$, toluene, 2M K_2CO_3, 110 °C, 3 d, (b) phenylboronic acid, 110 °C, 12 h, and (c) bromobenzene, 110 °C, 12 h; (*v*) (a) 3,6-bis(5-bromothiophen-2-yl)-2,5-bis(2-octyldodecyl)pyrrolo[3,4-*c*]pyrrole-1,4(2*H*,5*H*)-dione, 18-crown-6, Aliquat 336, $Pd(PPh_3)_4$, toluene, 2M K_2CO_3, 110 °C, 3 d, (b) phenylboronic acid, 110 °C, 12 h, and (c) bromobenzene, 110 °C, 12 h.

°C and stirred overnight. After cooling to room temperature, the mixture was poured into water and washed with ether. The combined organic extracts were dried with Na_2SO_4 and evaporated under vacuum. The residue was purified via silica gel chromatography (1:40 dichloromethane:hexanes) to yield a white powder (0.81 g, 38%). ^{1}H NMR (300 MHz, $CDCl_3$, δ): 7.97 (d, 2H, J = 9 Hz), 7.85 (d, 1H, J = 6 Hz), 7.58−7.68 (m, 2H), 7.35−7.50 (m, 4H), 2.53 (s, 3H). ^{13}C NMR (500 MHz, $CDCl_3$, δ): 130.8, 129.5, 125.9, 123.8, 121.7, 121.5, 118.87, 114.3, 113.0, 70.1, 69.2, 20.2.

Synthesis of 9-(4-Chloro-3-methylphenyl)-2,7-bis-(tetramethyl-1,3,2-dioxaborolan-2-yl)-9*H*-carbazole (2). Compound **1** (0.68 g, 1.5 mmol) was dissolved in THF (20 mL) and cooled to −78 °C. Then *n*-butyl lithium (1.26 mL, 3.1 mmol) was added dropwise. The solution was stirred for 1 h. Then, 2-isopropoxy-4,4,5,5-tetramethyl-1,3,2-dioxaborolane (0.59 g, 3.2 mmol) was added in one portion, and the mixture was allowed to warm to room temperature and stir overnight. The solution was then washed with water, dried with Na_2SO_4, and evaporated under vacuum. The residue was purified via silica gel chromatography (1:1 dichloromethane:hexanes) to yield a white powder (0.62 g, 76%). ^{1}H NMR (300 MHz, $CDCl_3$, δ): 8.18 (d, 2H, J = 6 Hz), 7.77 (d, 1H, J = 9 Hz), 7.75 (s, 2H), 7.61 (d, 1H, J = 6 Hz), 7.43 (s, 1H), 7.35 (d, 1H, J = 6 Hz), 2.52 (s, 3H), 1.38 (s, 24H). ^{13}C NMR (500 MHz, $CDCl_3$, δ): 141.1, 138.1, 136.0, 133.6, 130.6, 130.2, 126.7, 126.1, 125.5, 120.0, 116.0, 83.8, 24.9, 20.3.

Synthesis of CP Macromonomers. Compound **2** (10 mg, 0.02 mmol), $Ni(COD)_2$ (2.5 mg, 0.01 mmol), and triphenylphosphine (10 mg, 0.04 mmol) were dissolved in toluene (1 mL) in a glovebox. The mixture was heated to 50 °C and stirred at that temperature for 3 days. After cooling to room temperature, 1,3-bis(disphenylphosphino)-propane (11 mg, 0.025 mmol) was added and the solution was stirred at room temperature for 3 h. Meanwhile, 2-bromo-5-iodo-3-hexylthiophene was added to a Schlenk flask and dissolved in THF. After the mixture was cooled to 0 °C, isopropylmagnesium chloride was added dropwise and the solution was stirred for a further hour. Then, the catalyst solution was transferred out of the glovebox and injected into the thiophene monomer solution in a single portion. The ice bath was removed and the solution was warmed to room temperature and stirred for 5 h. Then 5 M HCl was added to quench the reaction. For CP(75) and CP(40), the solution was then poured into MeOH, the precipitate filtered. The polymers were then Soxhlet extracted with methanol (12 h), acetone (12 h), hexanes (12 h), and finally $CHCl_3$ (12 h). The $CHCl_3$ fraction was concentrated *in vacuo*, redissolved in $CHCl_3$, and precipitated in MeOH. CP(20) and CP(10) solutions were extracted with $CHCl_3$ and the residue was purified on a short silica gel column (50% dichloromethane:Hexanes to 100% dichloromethane) to yield the final macromonomers.

CP(10): Orange tacky solid. Yield: 27%. ^{1}H NMR (300 MHz, $CDCl_3$, δ): 8.20 (d, J = 6 Hz), 7.88 (s), 7.79 (d, J = 6 Hz), 7.70 (m), 7.48 (m), 7.45−7.30 (m), 7.10 (d, J = 9 Hz), 7.00 (m), 2.83 (m), 2.64 (s), 2.60 (m), 2.20 (t, J = 9 Hz), 1.70−1.60 (m), 1.5−1.3 (m), 0.93 (m).

CP(20): Red solid. Yield: 22%. ^{1}H NMR (300 MHz, $CDCl_3$, δ): 8.20 (d, J = 6 Hz), 7.87 (s), 7.75 (m), 7.70 (m), 7.49 (m), 7.45−7.30 (m), 7.10 (d, J = 9 Hz), 7.00 (m), 2.83 (m), 2.63 (s), 2.50 (m), 2.20 (t, J = 9 Hz), 1.75−1.60 (m), 1.5−1.3 (m), 0.94 (m).

CP(40): Dark solid. Yield: 65%. ^{1}H NMR (300 MHz, $CDCl_3$, δ): 8.20 (d, J = 6 Hz), 7.87 (s), 7.79 (d, J = 6 Hz), 7.72 (d, J = 9 Hz), 7.48 (m), 7.1 (m), 7.00 (s), 6.92 (m), 2.83 (t, J = 6 Hz), 2.64 (s), 1.73 (m), 1.5−1.3 (m), 0.94 (m).

CP(75): Dark solid. Yield: 71%. ^{1}H NMR (300 MHz, $CDCl_3$, δ): 8.20 (d, J = 6 Hz), 7.87 (s), 7.70 (m), 7.45 (mz), 7.26 (m), 7.00 (s), 2.83 (t, J = 6 Hz), 2.63 (m), 1.73 (m), 15−1.25 (m), 0.94 (m).

dx.doi.org/10.1021/ma5009435 | *Macromolecules* XXXX, XXX, XXX−XXX

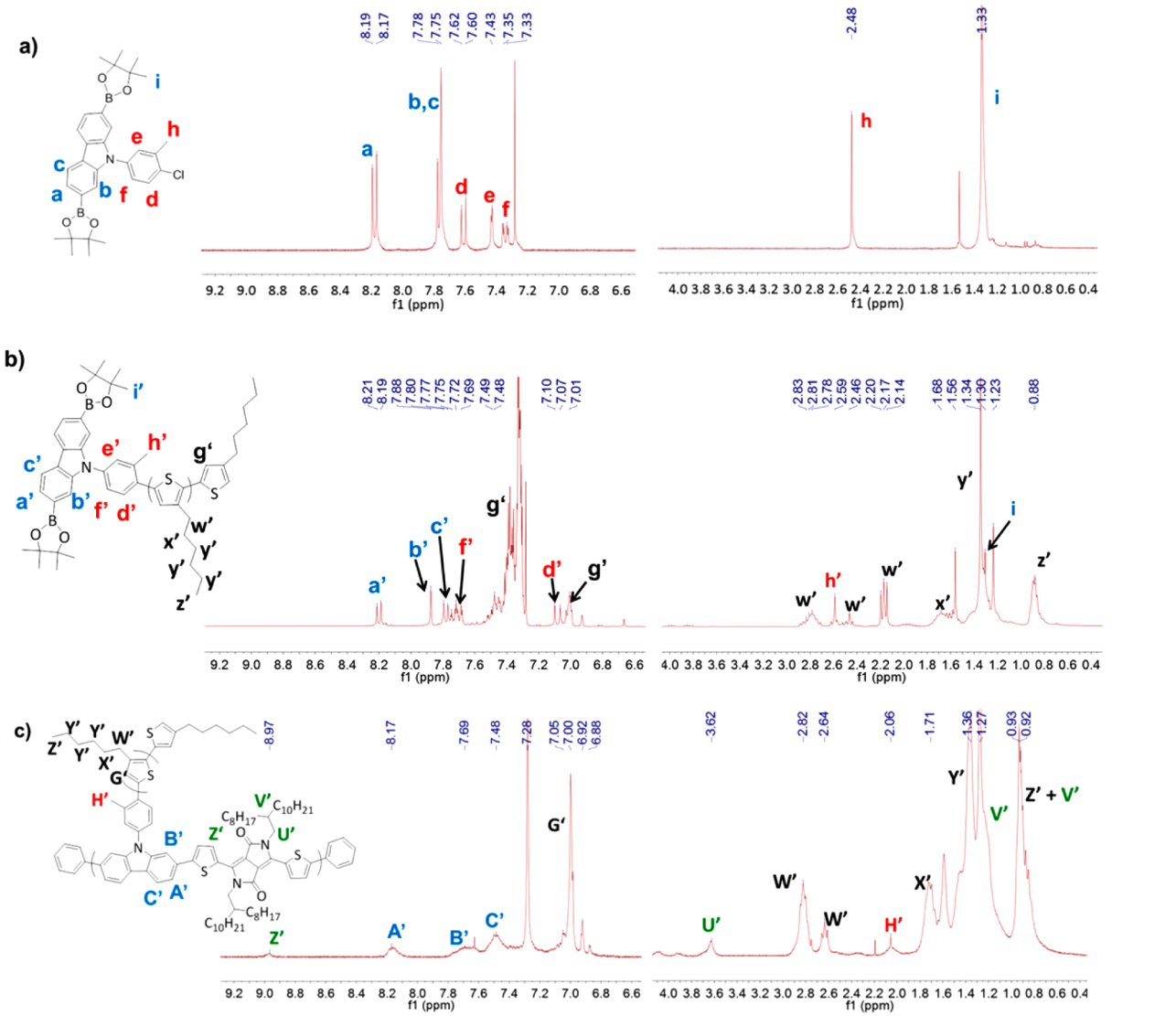

Figure 2. (a) ^{1}H NMR spectrum of carbazole initiator, (b) ^{1}H NMR spectrum of CP(20), and (c) ^{1}H NMR spectrum of CP(20)-DPP, with characteristic protons labeled.

Synthesis of CP-DPP Polymers. The appropriate CP macromonomer (1.0 mmol, based on M_n determined by MALDI−TOF for CP(10) and CP(20) or GPC for CP(40) and CP(75)), DPP monomer (1.0 mmol), 18-crown-6 (2.0 mmol), and Aliquat 336 (20 mol %) were added to a flask and degassed three times. Then, degassed toluene (5 mL) and 2 M K_2CO_3 (0.5 mL) were added, followed by $Pd(PPh_3)_4$ (5 mol %). The solution was heated to 110 °C and stirred for 3 days. The solution was cooled to room temperature and poured into MeOH. The precipitate was filtered and the polymers were then Soxhlet extracted with methanol (12 h), acetone (12 h), hexanes (12 h), and finally $CHCl_3$ (12 h). The $CHCl_3$ fraction was concentrated *in vacuo*, redissolved in $CHCl_3$, and precipitated in MeOH.

CP(10)-DPP: Dark solid. Yield: 73%. ^{1}H NMR (300 MHz, $CDCl_3$, δ): 9.00 (s), 8.20 (m), 7.75−7.40 (m), 6.99 (s), 6.92 (s), 2.82 (m), 2.64 (m), 2.06 (s), 1.80−1.10 (m), 0.93 (m).

CP(20)-DPP: Dark solid. Yield: 69%. ^{1}H NMR (300 MHz, $CDCl_3$, δ): 8.97 (s), 8.17 (m), 7.75−7.60 (m), 7.55−7.35 (m), 7.00 (s), 6.92 (s), 2.82 (t, J = 6 Hz), 2.64 (t, J = 6 Hz), 2.06 (s), 1.80−1.57 (m), 1.50−1.00 (m), 0.93 (m).

CP(40)-DPP: Dark solid. Yield: 86%. ^{1}H NMR (300 MHz, $CDCl_3$, δ): 8.97 (s), 8.20−8.10 (m), 7.80−7.60 (m), 7.55−7.40 (m), 7.00 (s), 6.92 (s), 2.82 (t, J = 6 Hz), 2.63 (t, J = 6 Hz), 2.06 (s), 1.80−1.55 (m), 1.50−1.00 (m), 0.93 (m).

CP(75)-DPP: Dark solid. Yield: 83%. ^{1}H NMR (300 MHz, $CDCl_3$, δ): 8.97 (s), 8.16 (m), 7.65−7.45 (m), 7.00 (s), 6.93 (s), 2.82 (t, J = 6 Hz), 2.06 (s), 1.80−1.60 (m), 1.50−1.20 (m), 0.93 (m).

Synthesis of 9-Phenyl-2,7-bis(4,4,5,5-tetramethyl-1,3,2-dioxaborolan-2-yl)-9*H*-carbazole (3). 9-Phenyl-2,7-dibromocarbazole (0.41 g, 1.0 mmol) was dissolved in THF (15 mL) and cooled to −78 °C. Then, *n*-butyl lithium (0.86 mL, 2.1 mmol) was added dropwise. The solution was stirred for 1 h. Then, 2-isopropoxy-4,4,5,5-tetramethyl-1,3,2-dioxaborolane (0.42 g, 2.2 mmol) was added in one portion and the mixture was allowed to warm to room temperature and stir overnight. The solution was then washed with water, dried with Na_2SO_4, and evaporated under vacuum. The residue was purified via silica gel chromatography (1:1 dichloromethane:hexanes) to yield a white powder (0.42 g, 83%). ^{1}H NMR (300 MHz, $CDCl_3$, δ): 8.16 (d, 2H, J = 6 Hz), 7.81 (s, 2H), 7.75 (d, 1H, J = 9 Hz), 7.65−7.50 (m, 1H, J = 6 Hz), 1.33 (s, 24H). ^{13}C NMR (500 MHz, $CDCl_3$, δ): 140.5, 138.6, 135.8, 131.1, 129.6, 128.9, 126.4, 125.5, 120.0, 116.0, 85.9, 25.1.

Synthesis of CbzDPP. Cbz monomer (0.24 g, 0.5 mmol), DPP monomer (0.49 g, 0.5 mmol), 18-crown-6 (0.256 g, 1.0 mmol), and Aliquat 336 (0.04 g, 0.1 mmol) were added to a flask and degassed three times. Then, degassed toluene (3 mL) and 2 M K_2CO_3 (0.25 mL) were added, followed by $Pd(PPh_3)_4$ (0.03 g, 0.02 mmol). The solution was heated to 110 °C and stirred for 3 days. The solution was cooled to room temperature and poured into MeOH. The precipitate

dx.doi.org/10.1021/ma5009435 | *Macromolecules* XXXX, XXX, XXX−XXX

was filtered and the polymer was Soxhlet extracted with methanol (12 h), acetone (12 h), hexanes (12 h), and finally $CHCl_3$ (12 h). The $CHCl_3$ fraction was concentrated *in vacuo*, redissolved in $CHCl_3$ and precipitated in MeOH to give a dark solid. Yield: 81%. ^{1}H NMR (300 MHz, $CDCl_3$, δ): 8.98 (s), 8.16 (br), 7.75−7.45 (m), 1.40−1.05 (m), 0.83 (m).

RESULTS AND DISCUSSION

Recent advances in externally initiated P3HT synthesis have allowed the introduction of functional groups on the terminus of P3HT, such as phosphonic acids.[30,31] Until recently, there had been no examples of Kumada catalyst transfer polycondensation (KCTP) as a tool to synthesize a fully conjugated graft copolymer. To the best of our knowledge, the first example was published by Wang et al. in the midst of the following studies.[32] In that publication, P3HT was grown from a naphthalene diimide (NDI)-thiophene copolymer, where a fraction of the thiophenes were functionalized with pendant chlorotoluene units. The grafted NDI-thiophene copolymer exhibited absorption and electronic traits of both the PNDI copolymer and P3HT. However, despite the n-type PNDI backbone, resultant OFET devices showed only p-type behavior with lower mobilities than either PNDI or P3HT.

The parent D−A copolymer from which to graft P3HT was chosen based on two requisites: (1) complementary absorption to P3HT and (2) minimal electronic communication between the backbone of the D−A copolymer and the P3HT chain. The former was important to realize broadband absorption, while the latter necessary to avoid conflation of the properties of the D−A copolymer and P3HT, or dominance of one set of traits over the other. Ultimately, a Cbz-DPP copolymer was chosen because it has an absorption max (λ_{max}) ca. 650 nm in solution[33] and a chlorotoluene initiator can easily be affixed to the Cbz group. In addition, it has been shown that there is little electron delocalization from the Cbz system to the pendant phenyl ring in *N*-phenylcarbazoles due to the torsional twist (ca. 60°) between the fused Cbz system and the pendant phenyl ring, as well as the partial break in conjugation through the central nitrogen.[34] It was hoped that this would preserve the individual characteristics of the D−A copolymer and P3HT in the final graft polymer, to avoid the conflation or dominance of the properties of the respective polymers. This break in conjugation is also important due to the limitations of the formation of the nickel catalyst complex used for external initiation. Previous studies have determined that including either electron-donating or electron-withdrawing functionalities *para* to the nickel site decreases the rate of oxidative addition and increases the likelihood of disproportionation reactions.[35]

The first attempt at graft polymer synthesis involved a "graft from" approach. First, the Cbz-DPP copolymer was synthesized using a novel Cbz monomer bearing a chlorotoluene P3HT initiator. Using traditional external initiation catalyst formation conditions, we attempted to form the *ex situ* nickel(II) catalyst. Unfortunately, ^{31}P NMR revealed that the oxidative addition reaction of the $Ni(COD)_2$ to the aryl−Cl bond did not occur. The addition did not occur at higher temperatures (50 °C) and extended times (3 days). It is supposed that the electronics of the Cbz-DPP copolymer hinder the oxidative addition reaction. It is also possible the steric congestion of the D−A copolymer slowed down the reaction.

At this juncture, it was of interest to determine if the oxidative addition could be accomplished using the boronic ester-functionalized Cbz monomer. Traditional *ex situ* catalyst formation conditions showed no evidence of the oxidative addition product. However, heating to 50 °C for 3 days promoted the reaction; the ^{31}P NMR spectrum (Figure S1, Supporting Information) shows a singlet occurring at 20 ppm, which is indicative of the oxidative addition product. The subsequent ligand exchange with 1.5 equiv of 1,3-dppp went rapidly after stirring for 2 h at room temperature, as confirmed by ^{31}P NMR (Figure S2). The spectrum also reveals the presence of $Ni(dppp)_2$, which likely forms from $Ni(PPh_3)_4$ remaining in solution as a result of the slow oxidative addition reaction. This solution was then injected into Grignardized 2-bromo-3-hexyl-5-iodothiophene (25 equiv to $Ni(COD)_2$) at 0 °C, warmed to room temperature, stirred for 5 h and finally quenched with 5 M hydrochloric acid. After precipitation and Soxhlet extraction, ^{1}H NMR revealed that P3HT was grown from the carbazole initiator (as shown by the shift in carbazole aromatic peaks and appearance of characteristic P3HT aromatic/aliphatic peaks) and the boronic esters were left intact to form the CP macromonomer (see Figure 2b as an example). It is important to note that the generation of catalytically inactive $Ni(dppp)_2$ skewed the calculated nickel:-monomer ratio, consistently yielding P3HT with 2-fold higher degree of polymerization (DP) than expected.

Unfortunately, thin layer silica (SiO_2) chromatography revealed the presence of nonexternally initiated P3HT as a result of these reactions. The most likely reason for this byproduct is disproportionation reactions during catalyst formation. Disproportionation reactions involve the exchange of ligands between two catalyst complexes and have been identified as a major source of side reactions during P3HT synthesis. *Para*-substituted aryl−$Ni(PPh_3)_2$−X complexes are known to be especially unstable to disproportionation.[36] If disproportionation is the source of the nonexternally initiated P3HT, it is likely occurring during the oxidative addition reaction when two $NiCbz(PPh_3)_2Cl$ complexes disproportionate to form $NiCbz_2(PPh_3)_2$ and $Ni(PPh_3)_2Cl_2$, which go on to form $NiCbz_2(dppp)$ and $Ni(dppp)Cl_2$. The latter complex is the catalyst historically used for P3HT synthesis, which would explain the presence of P3HT in the polymer mixture.[37]

With the confirmed synthesis of a CP macromonomer, the next step was to synthesize a series of CP macromonomers. Four macromonomers were synthesized with DP ranging from ∼10 (CP(10)) to ∼75 (CP(75)). To aid characterization of the macromonomers, CP(10) and CP(20) were purified on short SiO_2 columns to separate the carbazole-bound and free P3HT; CP(40) and CP(75) were too long to purify by column chromatography and were subjected to Soxhlet extraction, which necessarily meant that both CP and P3HT comprised the polymer mixture. The identity of the macromonomers was verified by ^{1}H NMR. In each case, the ^{1}H NMR spectra showed slight shifts for the aromatic carbazole protons and tolyl protons, verifying covalent P3HT attachment (Figure 2, parts a and b). Interestingly, the aromatic and alkyl thiophene peaks for the chromatographed CP and Soxhlet extracted CP are significantly different. Typically, ^{1}H NMR spectra of tolyl-initiated P3HT possesses a singlet at 7.00 ppm representing the P3HT aromatic proton and a triplet at ∼2.80 ppm corresponding to the two alkyl protons alpha to the thiophene rings.[38] These shifts are seen for the longer CP macromonomers (Figures S5 and S6). However, in the case of the chromatographed macromonomers (Figures S3 and S4), both the thiophene aromatic (7.30 to 7.45 ppm) and aliphatic (2.20 to 2.85 ppm) peaks exhibit a series of chemical shifts that

dx.doi.org/10.1021/ma5009435 | *Macromolecules* XXXX, XXX, XXX−XXX

appear to vary by the either the length of the P3HT chain or the proximity of the thiophene rings to the carbazole initiator. Similar NMR shifts that vary based upon the distance from a given proton to a functional group have been observed in other polythiophenes; for example, polythiophenes terminated with thiols, selenols, dithiocarbamates, and perfluoroalkyl chains experienced strong proximity-dependent NMR shifts.[39,40]

The DP of the macromonomers was estimated using ^{1}H NMR, GPC and MALDI−TOF. The DP was determined from the ^{1}H NMR spectra (Figures S3−S6) in an analogous way to the method published by Bronstein and Luscombe.[38] Unfortunately, it proved difficult to determine accurate integrations due to the overlapping peaks. As a way to corroborate these M_n values, gel permeation chromatography (GPC) was used. The GPC traces (Figure 3a) show a clear progression of the elution time for the four molecules, reflecting the decreasing DP of the macromonomers. Finally, the MALDI−TOF spectra (Figure 3b) of CP(10) and CP(20) reveal several insights. As expected, the peaks exhibit the weights of P3HT chains grown from boronic ester-functionalized carbazoles, which are 508.25 g/mol + (166.1 g/mol) × n + 1 g/mol, where n is the number of P3HT repeat units. In addition, the spectra show nearly complete end-group conversion following acid quenching, with negligible bromine-terminated chains. The estimated M_n of CP(10) and CP(20) based on the MALDI−TOF spectra were 8 and 12, respectively. Given the precise nature of MALDI−TOF, it is expected that the M_n values (Table 1) estimated from those spectra are the most accurate of the three methods used to determine DP. The MALDI−TOF spectra of CP(40) and CP(75) (not shown) inaccurately reflected the DP of the polymers. This could be due to the difficulty of volatilizing longer polymers. It has also been reported that MALDI−TOF is inaccurate for polymers with dispersities ($Đ$) > 1.40.[41] The estimated M_n of CP(10) and CP(20) based on the MALDI−TOF spectra were 8 and 12, respectively. Given the precise nature of MALDI−TOF, it is expected that the M_n values estimated from those spectra are the most accurate of the three methods used to determine DP. Both the NMR and GPC DP values were higher than the MALDI−TOF values. GPC has been reported to inflate the weights of conjugated polymers due to their rigid-rod structure compared to the polystyrene standard typically used to calibrate the GPC.[42] Also, determining the DP from ^{1}H NMR is inherently problematic as a result of the overlapping NMR peaks from 2.20 to 2.95 ppm, making the estimation imprecise. Regardless, the DP values are in rough agreement.

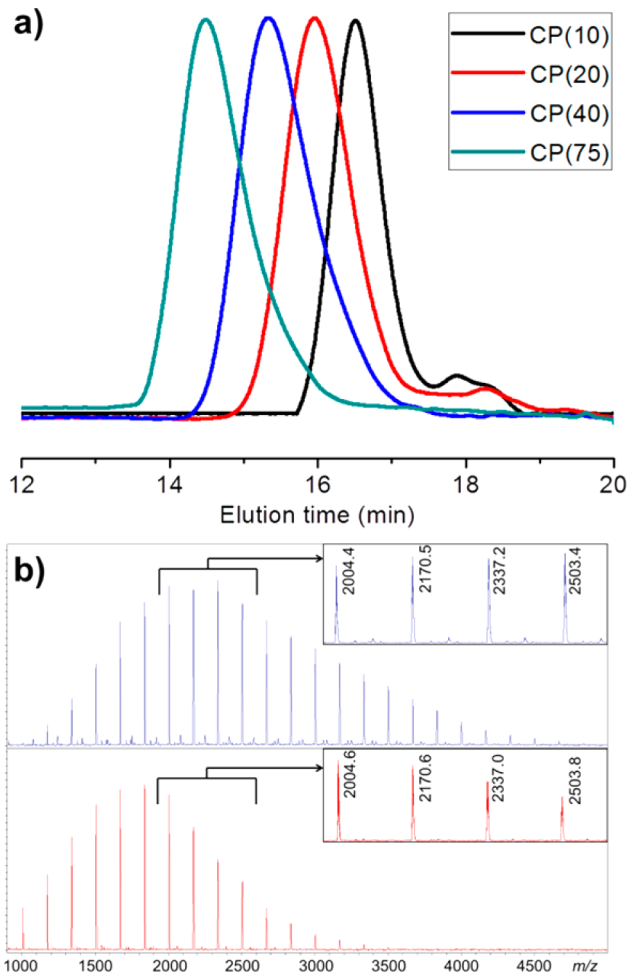

Figure 3. (a) GPC traces for macromonomers and (b) MALDI−TOF spectra for CP(20) (top) and CP(10) (bottom).

Following physical characterization, the optical and electronic properties of the macromonomers were probed using UV/vis spectroscopy and cyclic voltammetry (CV) (Table 2). The UV/vis spectra (Figure S7) showed two main transitions corresponding to the $\pi-\pi^*$ transitions of carbazole and P3HT at ∼310 nm and ∼450 nm, respectively. The P3HT peak experienced a progressive bathochromic shift as the DP increased, corresponding to the increase in conjugation length. Additionally, increasing the DP of P3HT resulted in a relatively less intense $\pi-\pi^*$ transition of carbazole. The CV spectra (Figure S8) show that as the macromonomer DP is increased, the highest occupied molecular orbital (HOMO) and LUMO increase and decrease, respectively, generating a smaller bandgap. This is an expected result of increasing the P3HT conjugation length, and corroborates the UV−vis spectra.

With this series of CP macromonomers in hand, the next step was to determine the conditions necessary for the graft through Suzuki polymerization. Initial attempts utilizing common Suzuki coupling conditions (refluxing toluene or THF, $Pd(PPh_3)_4$, 2 M K_2CO_3) yielded mainly starting monomers and some short oligomers. Increasing the reaction

Table 1. Physical, Optical, and Electronic Characterization of CP Macromonomers

polymer	$M_{n,GPC}$ (kDa)	$Đ_{GPC}$	$M_{n,NMR}$ (kDa)	$M_{n,MALDI-TOF}$ (kDa)	λ_{max} (nm)	$E_{ox}{}^a$ (V)	$E_{red}{}^b$ (V)	E_{HOMO} (eV)	E_{LUMO} (eV)
CP(10)	2.1	1.34	2.6	1.8	312	0.56	−1.75	−5.31	−3.00
CP(20)	4.1	1.41	4.4	2.8	439	0.51	−1.68	−5.26	−3.07
CP(40)	7.7	1.53	11.3	–	446	0.47	−1.63	−5.22	−3.12
CP(75)	13.3	1.51	15.4	–	451	0.44	−1.55	−5.19	−3.20

[a]As determined from oxidation onset found by cyclic voltammetry. [b]As determined from reduction onset found by cyclic voltammetry.

dx.doi.org/10.1021/ma5009435 | Macromolecules XXXX, XXX, XXX−XXX

Table 2. Physical, Optical, and Electronic Characterization of CP-DPP Graft Copolymers

polymer	M_n[a] (kDa)	PDI[a]	λ_{max}[b] (nm)	λ_{onset}[b] (nm)	$E_{g,ab}$[b] (eV)	E_{ox}[c] (V)	E_{red}[d] (V)	E_{HOMO} (eV)	E_{LUMO} (eV)	$E_{g,CV}$ (eV)
CP(10)-DPP	5.9	1.49	457, 694	855	1.45	0.57	−0.77	−5.32	−3.98	1.34
CP(20)-DPP	11.2	1.79	485, 637, 697	745	1.66	0.52	−1.17	−5.27	−3.58	1.69
CP(40)-DPP	12.4	2.23	507, 705	755	1.64	0.42	−1.57	−5.17	−3.18	1.99
CP(75)-DPP	28.3	2.72	522	650	1.91	0.41	−1.55	−5.16	−3.20	1.96
CbzDPP	6.3	1.61	649, 719	760	1.63	0.77	−0.75	−5.52	−4.00	1.52

[a]From gel permeation chromatography. [b]From thin film absorption measurements. [c]As determined from oxidation onset found by cyclic voltammetry. [d]As determined from reduction onset found by cyclic voltammetry.

duration had no effect on polymer formation. The use of phase-transfer catalysts (Aliquat 336) and water-miscible organic solvents with relatively high boiling points (dioxane) slightly improved the polymerization. However, 18-crown-6 was the single most important cocatalyst for the polymerization.

Subsequently, the four CP macromonomers were copolymerized with DPP using identical conditions, followed by Soxhlet extraction. A CbzDPP D−A copolymer was synthesized using the same conditions for reference. The resultant polymers were again characterized with ^{1}H NMR, GPC, MALDI−TOF, UV/vis spectroscopy and CV. The NMR spectrum of CP(20)-DPP (Figure 2c) exhibits a new peak at ∼9.0 ppm, representing the thiophene proton adjacent to the diketopyrrolopyrrole unit, which confirms the covalent attachment of the DPP monomer; this signal is also present in reference polymer CbzDPP and the other graft copolymers (Figure S9−S13). As can be seen from the CbzDPP spectrum, the multiplet of peaks from 7.30 to 7.75 ppm in the graft copolymer spectra arise from the carbazole moiety. Interestingly, the thiophene aromatic protons consistently shift upfield to 7.00 ppm for all the graft copolymers. Also, the series of multiplets in the CP(10) and CP(20) spectra from 2.20 to 2.95 ppm coalesce into a single triplet centered at 2.82 ppm in the spectra of CP(10)-DPP and CP(20)-DPP. Another notable feature of the NMR is the shift of the tolyl protons from 2.63 to 2.05 ppm. The ^{1}H NMR spectra for the graft copolymers show nearly identical shifts of the carbazole/P3HT aromatic/aliphatic protons and broadly similar features. Unfortunately, the integration of the DPP protons reveal that the DPP monomer is not incorporated stoichiometrically; generally, the carbazole to DPP ratio ranges from 2:1 to 4:1. This suggests that the graft polymerization did not work optimally. As predicted by the Carothers equation, the achievable DP of step-growth polymerizations are dictated by how precisely the monomers can be measured stoichiometrically. Both the difficulty of determining a precise molecular weight for the CP macromonomers and their Gaussian distribution of molecular weights make it unlikely to achieve maximal DP.

The GPC traces of the polymers exhibit a shoulder at shorter elution times, which are characteristic of higher molecular weight molecules created by step-growth polymerizations. CP(10)-DPP (Figure S14) and CP(20)-DPP (Figure 4) elute significantly more quickly than their precursor macromonomers; conversely, the elution profiles of CP(40)-DPP (Figure S15) and CP(75)-DPP (Figure S16) overlap more closely with that of their precursor macromonomers. These results can be explained by the fact that CP(40)-DPP and CP(75)-DPP contain P3HT from the macromonomer synthesis, which remains unmodified after the Suzuki polymerization.

The absorbance characteristics of the graft copolymers were characterized by UV−visible spectroscopy in solution (Figure 5) and thin film (Figure S18), with the solution spectrum of the

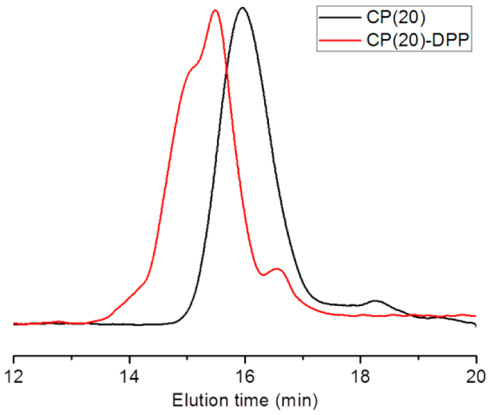

Figure 4. GPC elution profiles for CP(20) and CP(20)-DPP.

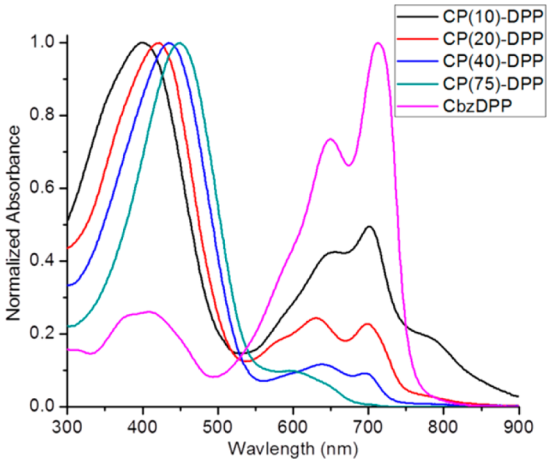

Figure 5. UV−visible $CHCl_3$ solution spectra for CP-DPP graft copolymers, with CbzDPP donor−acceptor absorbance for reference.

CbzDPP copolymer for reference in each case. Generally, each graft copolymer possesses a P3HT $\pi-\pi^*$ transition around 400−450 nm and a CbzDPP donor−acceptor ICT peak from 550 to 800+ nm. The ICT peak of the linear CbzDPP polymer has two main peaks (ca. 650 and 710 nm), which is also reflected in the bimodal ICT peaks of the graft copolymers, except CP(75)-DPP, which shows a small ill-defined ICT peak. Thus, as hypothesized, the carbazole produces a sufficient break in conjugation to realize the optical properties of both components.

There is a clear trend in the intensity, shape and onset of the ICT peak in the graft copolymers as the P3HT length is varied. As the P3HT side chain was shortened, the ratio of the P3HT $\pi-\pi^*$ transition intensity to the donor−acceptor ICT peak decreased; conversely, the longer P3HT chains resulted in a more intense P3HT $\pi-\pi^*$ transition. This phenomenon is

dx.doi.org/10.1021/ma5009435 | Macromolecules XXXX, XXX, XXX−XXX

similar to the inverse relationship seen between the carbazole and P3HT absorption intensities in the macromonomers. There could be several explanations for this. First and foremost, the CP(40)-DPP and CP(75)-DPP polymers contain P3HT which accounts for some of their absorption around 450 nm. As stated above, this P3HT also results in nonequimolar monomers, which limits the polymerization length and the resultant ICT intensity. It is also possible that the relative amount of P3HT and donor−acceptor polymer dictates the absorption profile—i.e., as the P3HT chain becomes shorter and the $\pi-\pi^*$ transition becomes weaker, the donor−acceptor peak becomes more prominent and *vice versa*. The longer CP macromonomers undoubtedly produce more steric congestion during the Suzuki polymerization and limit the length of the donor−acceptor polymer.

Regardless, there is clearly an inverse relationship between the length of the CP macromonomers and the onset and relative intensity of the ICT peak in the graft copolymers. This trend is supported by results from recent studies on D−A copolymers incorporating thienylated benzodithiophene donors, which have shown that adding two or three pendant thiophene rings to the donor generates an increasingly strong electronic transition around 400 nm.[43] Also of interest is that the ICT peaks of CP(10)-DPP and CP(20)-DPP both exhibit a shoulder at longer wavelengths. Thin film absorbance showed similar trends compared to the solution measurements, with slight broadening of the peaks and bathochromic shifts of both the P3HT $\pi-\pi^*$ transition and ICT peaks.

The electronic behavior and energy levels of the graft copolymers were further investigated by CV (Figure 6). The

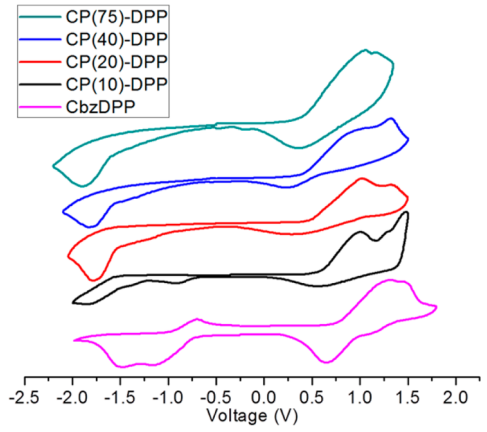

Figure 6. Cyclic voltammetry of CP-DPP graft copolymers and CbzDPP.

formation of the CbzDPP backbone changes the electronics of the graft polymers compared to their macromonomers. Generally, each graft copolymer exhibits electronic characteristics of both P3HT and CbzDPP, with the electronic processes of P3HT being much more significant than those of CbzDPP. Additionally, the greater the relative proportion of CbzDPP in the final graft copolymer, the more drastic the changes in the CV scan contours. Thus, while the scans for CP(75)-DPP appear nearly identical to the CP(75) macromonomer scans in both shape and position, the copolymers with shorter P3HT chains showed significant departure from their macromonomer CV scans. In all cases, the redox processes of P3HT and CbzDPP seem to be largely independent from each other. For example, both CP(10)-DPP and CbzDPP have reduction onsets that are nearly identical and possess two reduction peaks ca. −0.75 and −1.25 V. However, CP(10)-DPP still exhibits a large P3HT reduction at nearly the same potential as the CP(10) macromonomer. The covalent attachment of DPP has a much smaller effect on the reduction scans of the other graft copolymers, appearing as a slight change in the slope of the reduction curve; this change of slope is nearly absent from CP(75)-DPP. The onset oxidation potentials of the graft copolymers are nearly identical to those of their respective macromonomer. This can be explained by the fact that the P3HT oxidation occurs at lower potentials than carbazole, so the onset potential of the graft copolymer is dictated by the P3HT chain. Unlike the macromonomers, the graft copolymers all have two or more quasi-reversible oxidation events, presumably corresponding to the sequential oxidation of the P3HT side chains and CbzDPP backbones. Finally, the band gap energies calculated from the oxidation/reduction onsets are in rough agreement with the band gap energies calculated from the thin film absorption onsets. The one exception is that of CP(40)-DPP; although the UV−vis spectrum shows a clear ICT peak, the reduction is so slight in the CV spectrum that the P3HT reduction potential was used to calculate the LUMO level.

The thermal behaviors of the polymers were characterized by differential scanning calorimetry (DSC). Figure 7 shows typical

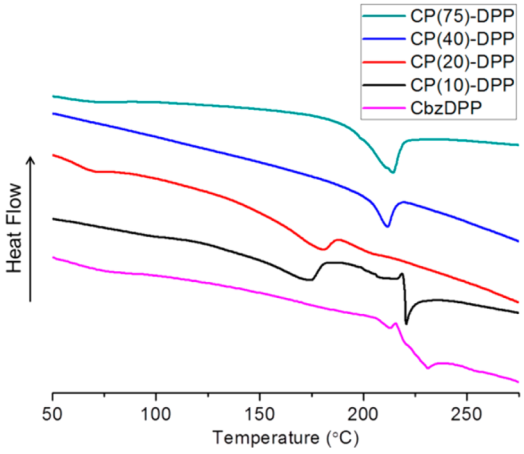

Figure 7. Differential scanning calorimetry of CP-DPP graft copolymers and CbzDPP.

thermograms of each material. CbzDPP shows a melting point (T_m) of 231 °C. The CP-DPP polymers show decreasing P3HT T_m of 217, 211, 180, and 174 °C with decreasing P3HT length. It is known that longer P3HT chains exhibit stronger intermolecular interactions than shorter P3HT chains, which would explain the increasing T_m values with increasing molecular weight.[44] This stronger intermolecular interaction is also reflected in the thin film absorption spectra. As the P3HT chain increases in length, there appears a more defined low-energy vibronic shoulder on the main P3HT $\pi-\pi^*$ transition, which results from ordered packing in the solid state. Also of note is that CP(10)-DPP possesses a second T_m at 215 °C, which is likely due to the higher proportion of CbzDPP in the final graft polymer.

Finally, the free-charge carrier mobilities of each polymer were determined from organic field effect transistors (OFETs) and the microstructures of the optimized OFETs were characterized by atomic force microscopy (AFM). To fabricate

dx.doi.org/10.1021/ma5009435 | *Macromolecules* XXXX, XXX, XXX−XXX

optimized OFET devices, the spin-coating solvent, spin-coating speed, and annealing temperature were varied. Optimized devices were processed from chloroform, spun at 2000 rpm, with the graft copolymers and CbzDPP being annealed at 65 and 155 °C, respectively. AFM images and the OFET transfer and output curves for CP(75)-DPP, CP(10)-DPP, and CbzDPP are shown in Figures S19−S23.

The optimized OFET mobilities seem to reflect the polymer composition. The device properties of the graft polymers with P3HT suffered relative to those of the neat CbzDPP polymer. Both CP(10)-DPP and CbzDPP exhibit similar ambipolar properties, with the addition of the small amount of P3HT only slightly reducing the hole mobility from $7 \times 10^{-3} \pm 2 \times 10^{-3}$ $cm^2\ V^{-1}\ s^{-1}$ for CbzDPP to $5 \times 10^{-3} \pm 3 \times 10^{-3}$ $cm^2\ V^{-1}\ s^{-1}$ for CP(10)-DPP. They both have similar electron mobilities of $7 \times 10^{-4} \pm 2 \times 10^{-4}$ $cm^2\ V^{-1}\ s^{-1}$ for CbzDPP and $7 \times 10^{-4} \pm 3 \times 10^{-4}$ $cm^2\ V^{-1}\ s^{-1}$ for CP(10)-DPP. The surface morphology of these materials shows reduced domain sizes for CP(10)-DPP relative to CbzDPP, as expected due to an increase in disorder in the P3HT containing system. Further increasing the concentration of P3HT to CP(20)-DPP and CP(40)-DPP results in devices that do not work well for transistor applications, with CP(20)-DPP not turning on and CP(40)-DPP resulting in devices with barely measurable output curves (not shown). Further increasing the P3HT concentration to CP(75)-DPP results in p-type transistors with mobilities of $6 \times 10^{-4} \pm 1 \times 10^{-4}$ $cm^2\ V^{-1}\ s^{-1}$. This likely arises due to favorable $\pi-\pi$ interactions between the longer P3HT chains, and minimal contribution from the CbzDPP copolymer. These films also show domains with dimensions similar to those of CP(10)-DPP. Overall, it appears that there is a general trend of transport properties being derived from the CbzDPP backbone with short P3HT chains, followed by a disruption in the electronic structure with increasing P3HT lengths, before the transport properties become dominated by P3HT interactions.

CONCLUSION

In conclusion, a synthetic methodology was pioneered and optimized to realize the first example of a "graft through" approach to attain conjugated graft copolymers. In addition, a new carbazole-based external initiating moiety was discovered for P3HT synthesis, which resulted in controllable growth of P3HT. A Suzuki polymerization involving this carbazole-P3HT macromonomer and a diketopyrrolopyrrole acceptor was optimized. Thereafter, four iterations of a carbazole-P3HT-diketopyrrolopyrrole graft copolymer were synthesized, differing by the degree of polymerization of the P3HT chain. The final polymers exhibit two major absorption peaks due to the P3HT $\pi-\pi^*$ transition and ICT between carbazole and diketopyrrolopyrrole units. Moreover, the relative intensities of peaks were proportional to the relative amount of P3HT and donor−acceptor copolymer.

Clearly, the main two drawbacks of this approach are (1) the conditions required to realize the oxidative addition reaction during the *ex situ* catalyst formation and (2) the mandatory use of a graft through polymerization. Both of these limitations are a result of the initiator design. The functionalized carbazole has a large electronic effect at the site of the oxidative addition, thereby disfavoring the reaction. In the case of the boronic−ester-functionalized carbazole, this generates byproducts during catalyst formation and ultimately leads to a P3HT impurity, as well as P3HT lengths that differ significantly from the predicted lengths; conversely, in the case of the graft from approach, the carbazole−diketopyrrolopyrrole D−A polymer is sufficient to completely retard the oxidative addition reaction. Unfortunately, the graft from approach is preferable to the graft through approach in this system because of the nature of step-growth and chain-growth polymeriations. The macromonomers for the graft through approach necessarily have a Gaussian distribution of molecular weights, which makes achieving a perfect 1:1 stoichiometric ratio during the Suzuki polymerization nearly impossible. This thereby limits the efficiency and reproducibility of the Suzuki polymerization. If such systems could be designed to improve the efficiency of the catalyst formation and P3HT grafting reaction, it would be interesting to utilize other conjugated molecules as initiators in P3HT synthesis to probe the way they affect the optical, electronic, and self-assembly properties of conjugated materials.

ASSOCIATED CONTENT

Supporting Information

NMR spectra, CV scans, GPC plots, UV−vis spectra, AFM images, and OFET output and transfer curves of the Ni catalyst, macromonomers, and graft copolymers. This material is available free of charge via the Internet at http://pubs.acs.org.

AUTHOR INFORMATION

Corresponding Author

*(C.K.L.) E-mail: luscombe@u.washington.edu.

Notes

The authors declare no competing financial interest.

ACKNOWLEDGMENTS

This work was supported by the NSF (EFRI-SEED 1038165 and DMR 1407815) and by the State of Washington through the University of Washington Clean Energy Institute.

REFERENCES

(1) Polman, A.; Atwater, H. A. *Nat. Mater.* **2012**, *11*, 174.
(2) P. Würfel *Physics of Solar Cells*; Wiley-VCH: Weinheim, Germany, 2004.
(3) Ameri, T.; Li, N.; Brabec, C. J. *Energy Environ. Sci.* **2013**, *6*, 2390−2413.
(4) Riede, M.; Uhrich, C.; Widmer, J.; Timmreck, R.; Wynands, D.; Schwartz, G.; Gnehr, W.-M.; Hildebrandt, D.; Weiss, A.; Hwang, J.; Sundarraj, S.; Erk, P.; Pfeiffer, M.; Leo, K. *Adv. Funct. Mater.* **2011**, *21*, 3019−3028.
(5) You, J.; Dou, L.; Yoshimura, K.; Kato, T.; Ohya, K.; Moriarty, T.; Emery, K.; Chen, C.-C.; Gao, J.; Li, G.; Yang, Y. *Nat. Commun.* **2013**, *4*, 1−10.
(6) Kim, J. Y.; Lee, K.; Coates, N. E.; Moses, D.; Nguyen, T.-Q.; Dante, M.; Heeger, A. J. *Science.* **2007**, *317*, 222−225.
(7) Dennler, G.; Scharber, M. C.; Ameri, T.; Denk, P.; Forberich, K.; Waldauf, C.; Brabec, C. J. *Adv. Mater.* **2008**, *20*, 579−583.
(8) Yang, J.; Zhu, R.; Hong, Z.; He, Y.; Kumar, A.; Li, Y.; Yang, Y. *Adv. Mater.* **2011**, *23*, 3465−3470.
(9) Jo, J.; Pouliot, J.-R.; Wynands, D.; Collins, S. D.; Kim, J. Y.; Nguyen, T. L.; Woo, H. Y.; Sun, Y.; Leclerc, M.; Heeger, A. J. *Adv. Mater.* **2013**, *25*, 4783−4788.
(10) Li, K.; Li, Z.; Feng, K.; Xu, X.; Wang, L.; Peng, Q. *J. Am. Chem. Soc.* **2013**, *135*, 13549−13557.
(11) Meiss, J.; Menke, T.; Leo, K.; Uhrich, C.; Gnehr, W.-M.; Sonntag, S.; Pfeiffer, M.; Riede, M. *Appl. Phys. Lett.* **2011**, *99*, 043301.
(12) Dennler, G.; Prall, H.-J.; Koeppe, R.; Egginger, M.; Autengruber, R.; Sariciftci, N. S. *Appl. Phys. Lett.* **2006**, *89*, 073502.
(13) You, J.; Dou, L.; Yoshimura, K.; Kato, T.; Ohya, K.; Moriarty, T.; Emery, K.; Chen, C.-C.; Gao, J.; Li, G.; Yang, Y. *Nat. Commun.* **2013**, *4*, 1446.

(14) Green, M. A.; Emery, K.; Hishikawa, Y.; Warta, W.; Dunlop, E. D. *Prog. Photovoltaics* **2013**, *21*, 1.
(15) Yang, L.; Yan, L.; You, W. J. *Phys. Chem. Lett.* **2013**, *11*, 1802−1810.
(16) Cheng, P.; Li, Y.; Zhan, X. *Energy Environ. Sci.* **2014**, *7*, 2005−2011.
(17) Khlyabich, P. P.; Burkhart, B.; Thompson, B. C. *J. Am. Chem. Soc.* **2011**, *133*, 14534−14537.
(18) Street, R. A.; Davies, D.; Khlyabich, P. P.; Burkhart, B.; Thompson, B. C. *J. Am. Chem. Soc.* **2013**, *135*, 986−989.
(19) Hesse, H. C.; Weickert, J.; Hundschell, C.; Feng, X.; Müllen, K.; Nickel, B.; Mozer, A. J.; Schmidt-Mende, L. *Adv. Energy Mater.* **2011**, *1*, 861−869.
(20) Hu, Z.; Tang, S.; Ahlvers, A.; Khondaker, S. i.; Gesquiere, A. J. *Appl. Phys. Lett.* **2012**, *101*, 053308.
(21) Koppe, M.; Egelhaaf, H. J.; Dennler, G.; Scharber, M. C.; Brabec, C. J.; Schilinsky, P.; Hoth, C. N. *Adv. Funct. Mater.* **2010**, *20*, 338.
(22) Ameri, T.; Khoram, P.; Min, J.; Brabec, C. J. *Adv. Mater.* **2013**, 1−22.
(23) Kroon, R.; Lenes, M.; Hummelen, J. C.; Blom, P. W. M.; De Boer, B. *Polym. Rev.* **2008**, *48*, 531.
(24) Nam, C.-Y.; Wu, Q.; Su, D.; Chiu, C.-Y.; Tremblay, N. J.; Nuckolls, C.; Black, C. T. *J. Appl. Phys.* **2011**, *6*, 064307.
(25) Segura, J. L.; Martin, N.; Guldi, D. M. *Chem. Soc. Rev.* **2005**, *34*, 31−47.
(26) Wang, M.; Wudl, F. *J. Mater. Chem.* **2012**, *22*, 24297−24314.
(27) Jiang, W.; Duan, L.; Qiao, J.; Dong, G.; Zhang, D.; Wang, L.; Qiu, Y. *J. Mater. Chem.* **2011**, *21*, 4918−4926.
(28) Letizia, J. A.; Salata, M. R.; Tribout, C. M.; Facchetti, A.; Ratner, M. A.; Marks, T. J. *J. Am. Chem. Soc.* **2008**, *130*, 9679−9694.
(29) Lee, O. P.; Yiu, A. T.; Beaujuge, P. M.; Woo, C. H.; Holcombe, T. W.; Millstone, J. E.; Douglas, J. D.; Chen, M. S.; Fréchet, J. M. J. *Adv. Mater.* **2011**, *23*, 5359−5363.
(30) Doubina, N.; Jenkins, J. L.; Paniagua, S. A.; Mazzio, K. A.; MacDonald, G. A.; Jen, A. K.-Y.; Armstrong, N. R.; Marder, S. R.; Luscombe, C. K. *Langmuir.* **2012**, *28*, 1900−1908.
(31) Doubina, N.; Paniagua, S. A.; Soldatova, A. V.; Jen, A. K.-Y.; Marder, S. R.; Luscombe, C. K. *Macromolecules.* **2011**, *44*, 512−520.
(32) Wang, J.; Lu, C.; Mizobe, T.; Ueda, M.; Chen, W.-C.; Higashihara, T. *Macromolecules.* **2013**, *46*, 1783−1793.
(33) Zou, Y.; Gendron, D.; Badrou-Aïch, R.; Najari, A.; Tao, Y.; Leclerc, M. *Macromolecules.* **2009**, *42*, 2891−2894.
(34) Kwon, O.; Barlow, S.; Odom, S. A.; Beverina, L.; Thompson, N. J.; Zojer, E.; Brédas, J.-L.; Marder, S. R. *J. Phys. Chem. A* **2005**, *109*, 9346−9352.
(35) Doubina, N.; Ho, A.; Jen, A. K.-Y.; Luscombe, C. K. *Macromolecules* **2009**, *42*, 7670−7677.
(36) Kiriy, A.; Senkovskyy, V.; Sommer, M. *Macromol. Rapid Commun.* **2011**, *32*, 1503−1517.
(37) Osaka, I.; McCullough, R. D. *Acc. Chem. Res.* **2008**, *41*, 1202−1214.
(38) Bronstein, H.; Luscombe, C. K. *J. Am. Chem. Soc.* **2009**, *131*, 12894−12895.
(39) Mao, Z.; Vakhshouri, K.; Jaye, C.; Fischer, D. A.; Fernando, R.; DeLongchamp, D. M.; Gomez, E. D.; Sauvé, G. *Macromolecules* **2013**, *46*, 103−112.
(40) Okamoto, K.; Luscombe, C. K. *Chem. Commun.* **2014**, *50*, 5310−5312.
(41) Wetzel, S. J.; Guttman, C. M.; Flynn, K. M.; Filliben, J. J. *J. Am. Soc. Mass Spectrom.* **2006**, *17*, 246−252.
(42) Khan, M. S.; Al-Mandhary, M. R. A.; Al-Suti, M. K.; Ahrens, B.; Mahon, M. F.; Male, L.; Raithby, P. R.; Boothby, C. E.; Köhler, A. *Dalton Trans.* **2003**, *24*, 74−84.
(43) Kuo, C.-Y.; Nie, W.; Tsai, H.; Yen, H.-J.; Mohite, A. D.; Gupta, G.; Dattelbaum, A. M.; William, D. J.; Cha, K. C.; Yang, Y.; Wang, L.; Wang, H.-L. *Macromolecules* **2014**, *47*, 1008−1020.
(44) Zen, A.; Pflaum, J.; Hirschmann, S.; Zhuang, W.; Jaiser, F.; Asawapirom, U.; Rabe, J. P.; Scherf, U.; Neher, D. *Adv. Funct. Mater.* **2004**, *14*, 757−764.